Detecting nighttime inversions in the interior of a Douglas fir canopy

Schilperoort, Bart; Coenders-Gerrits, Miriam; Jiménez Rodríguez, César; van Hooft, Antoon; van de Wiel, Bas; Savenije, Hubert

Important note
To cite this publication, please use the final published version (if applicable).
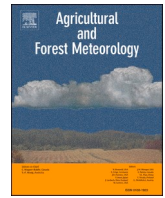Please check the document version above.

Detecting nighttime inversions in the interior of a Douglas fir canopy

Bart Schilperoort [a],[*], Miriam Coenders-Gerrits [a], César Jiménez Rodríguez [a],[c],
Antoon van Hooft [b], Bas van de Wiel [b], Hubert Savenije [a]

[a] *Delft University of Technology, Water Management department, Stevinweg 1, 2628, CN, Delft, the Netherlands*
[b] *Delft University of Technology, Geoscience & Remote Sensing department, Stevinweg 1, 2628, CN, Delft, the Netherlands*
[c] *Luxembourg Institute of Science and Technology, Av. des Hauts-Fourneaux, 4362, Esch-sur-Alzette, Luxembourg*

ABSTRACT

Despite the importance of forests in the water and carbon cycles, accurately measuring their contribution remains challenging, especially at night. During clear-sky nights current models and theories fail, as non-turbulent flows and spatial heterogeneity become more important. One of the standing issues is the 'decoupling' of the air masses in and above the canopy, where little turbulent exchange takes place, thus preventing proper measurement of atmospheric fluxes. Temperature inversions, where lower air is colder and thus more dense, can be both the cause and result of this decoupling.

With Distributed Temperature Sensing (DTS) it is now possible to detect these temperature inversions, and increase our understanding of the decoupling mechanism. With DTS we detected strong inversions within the canopy of a tall Douglas Fir stand. The inversions formed in on clear-sky nights with low turbulence, and preferentially formed in the open understory. A second inversion regularly occurred above the canopy. Oscillations in this upper inversion transferred vertically through the canopy and induced oscillations in the lower inversion.

We hypothesize that the inversions could form due to a local suppression of turbulent motions along the height of the canopy. This was supported by a 1-D conceptual model, which showed that a local inversion layer would always form within the canopy if the bulk inversion (over the full canopy) was strong enough.

Due to the near-continuous vertical motion and specific height the inversions occur at, a very high measurement density (better than ~2 m) and measurement frequency (>0.1 Hz) are required to detect them. Consequently, it could be possible that the observed inversions are a regular feature in similarly structured forests, but are generally not directly observed. With DTS it is possible to detect and describe these types of features, which will aid in improving our understanding of atmospheric flows over complex terrain such as forests.

1. Introduction

Forests cover a large area of the earth's land surface and form important components of both the water and the carbon cycle. However, due to their intrinsic height scale and complexity, measuring their contribution to these cycles has remained very challenging (Wilson, 2002; Barr et al., 1994). In particular during nighttime, when fluxes are modest in magnitude, measuring exchange of carbon dioxide, water vapor, and heat between the forest canopy and atmosphere is difficult.

During the day, strong convection will ensure strong mixing of air which enables frequent exchange of air masses between the forest and the atmosphere above. Likewise, high wind conditions favor such

exchange. In contrast, during low wind and clear-sky nights current models and theories fail, as non-turbulent flows and spatial heterogeneity becomes more dominant (Katul et al., 1995). An issue affecting nighttime measurements specifically in forests is decoupling; a lack of turbulent exchange between the canopy and the atmosphere (Aubinet et al., 2012). This lack of turbulent exchange makes experimental quantification of water, carbon, and energy fluxes above forests difficult, as measurements above the canopy are not representative for what is happening inside the canopy (Jocher et al., 2017). Decoupling is caused by the lack of generation of turbulence due to the absence of sufficient wind shear, and also due to the suppression of turbulence by stable stratification; when the canopy, or parts of it, are colder than the
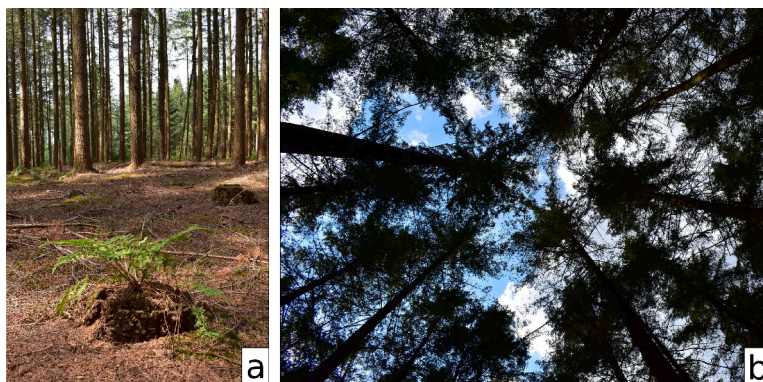
Fig. 1. Photos illustrating the bare forest floor (a), and the canopy structure (b) at the Speulderbos study site. (Schilperoort et al., 2020).
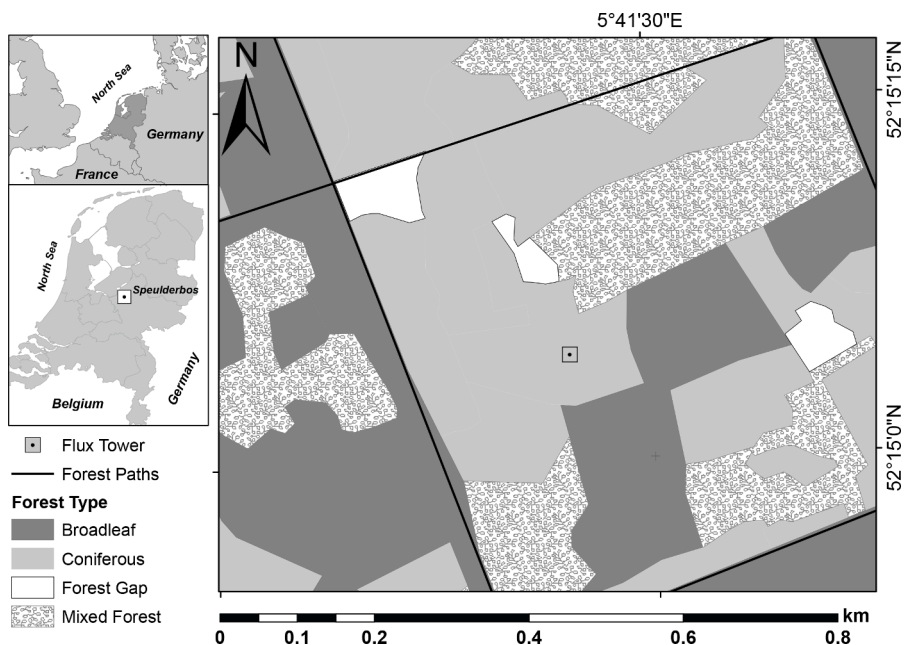

Fig. 2. Forest type distribution around the tower site at the Speulderbos forest, the Netherlands (Schilperoort et al., 2018).

atmosphere above (Baldocchi and Meyers, 1988; Thomas et al., 2017; Schilperoort et al., 2020). If not taken into account, decoupling will affect the interpretation of forest fluxes such as water and CO_2 (Fitz-jarrald and Moore, 1990; Alekseychik et al., 2013).

There are different (proxy) methods to assess whether the canopy is in a decoupled state or not. So-called u_* (friction velocity) filtering is often used to filter flux data for periods with low wind shear (Goulden et al., 1996; Papale et al., 2006; Barr et al., 2013). Other methods use the relationship between the standard deviation of vertical wind speed (σ_w), both above and below the canopy (Thomas et al., 2013), or look at (cross-)correlation between the measurements of vertical wind speeds (Cava and Katul, 2009; Jocher et al., 2020). However, the above methods are only proxies for the momentum exchange, and do not actually detect the density stratification over the full canopy-atmosphere continuum. By detecting such stratification one could assess whether indeed temperatures vary smoothly with height or that 'separated' or 'decoupled' layers are being formed.

Besides it has to be realized that decoupling is not a binary state. A range of different exchange regimes can occur, from a fully coupled canopy, to a decoupled subcanopy, to lastly a fully decoupled canopy (Göckede et al., 2007). Strong temperature inversions, where air lower down is colder and thus denser than air above, within or over the canopy, can both affect as well as be the result of the decoupling. By

knowing if such an inversion exists, and at which height it is, the degree of coupling of a canopy can be studied in much more detail. In this study therefore, we present high-resolution (~0.3 m) observations of in-canopy temperature using the so-called DTS technique.

Distributed Temperature Sensing (DTS) is a measurement technique that has found increasing use in atmospheric measurements, for measuring air temperature (Thomas et al., 2012; Zeeman et al., 2015; Izett et al., 2019; Peltola et al., 2020) as well as wind speed profiles (van Ramshorst et al., 2019; Lapo et al., 2020). DTS measurements are made by shining a laser down a fiber optic (FO) cable, and analyzing the Raman backscatter signal. As this Raman backscatter is only sensitive to temperature, the temperature along the entire FO cable can be moni-tored continuous in space (Smolen and van der Spek, 2003; Hartog, 2017). This is akin to having a long string of standard temperature sensors. In a previous study by Schilperoort et al. (2020) decoupling was investigated in a Douglas fir canopy with the use of a DTS measured vertical temperature profile. It was hypothesized that a 'blocking layer' existed within the understory, which reduces the turbulent exchange between the forest floor and the rest of the canopy. A drawback in their data analysis was that the data had high spatial resolution (30 cm) but that it was limited in its temporal resolution. This was due to the type of FO cables used: thick cables which respond slowly to changes in air temperature. To expand on this study, an adjusted measurement setup
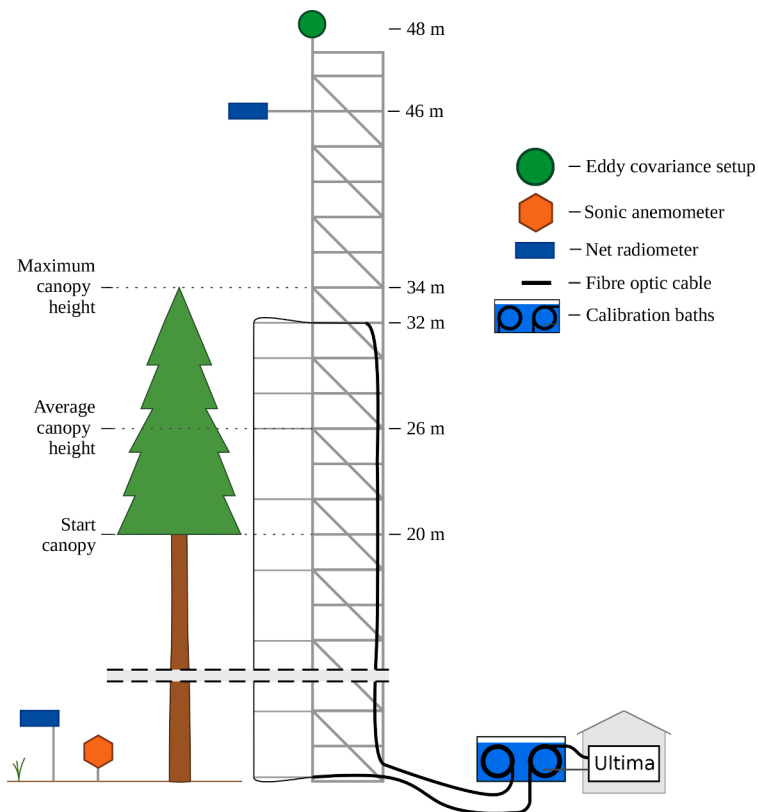
Fig. 3. Schematic overview of the measurement setup at the tower.

was placed on the site, which is capable to detect air temperature variations at a high frequency (~0.5 Hz). This enables us to make more definitive conclusions about the nature of the blocking layer and to detect dynamical features such as internal gravity waves.

Using these high frequency air temperature profiles, we will look at the presence of temperature inversions within the Douglas Fir canopy. We will study their formation and distribution within the canopy, and look at inversion dynamics at different scales. Next we will discuss the reasons why these inversions within the canopy can often elude detection, i.e., why they are not observed more often using more traditional point sensors. Finally, to explain why and under which conditions the inversions form, we present a simple 1-D conceptual model to support our hypothesis on the mechanism behind the layer formation within the canopy.

2. Materials and Methods

2.1. Study Site

The measurements were performed at the Speulderbos study site in the Netherlands (52°15'N, 5°41'E, Fig. 2). The forest surrounding the field site consists of patches of different tree types, both planted and native trees in different succession stages, intersected by access roads. The patch in which the flux tower is located consists of Douglas Fir trees (Pseudotsuga menziesii), planted in 1962, with a mean canopy height of around 34 m (Cisneros Vaca et al., 2018). The Douglas Fir trees form a very dense canopy from 20 – 30 meters, while the bottom 20 m of the stand is completely bare, apart from the trunks (Fig. 1). This can also be seen in the vertical distribution of the Plant Area Index (PAI, Appendix C). The forest floor is mostly covered in a layer of needles, with only limited undergrowth present (e.g., ferns, mosses). A more detailed description of the canopy structure can be found in Schilperoort et al. (2020). The site is located on a hillslope, with a local grade of ~2.5%. The surrounding area varies in slope (Appendix B).

2.2. Setup

To measure a vertical profile of air temperature, a thin fiber optic (FO) cable was placed vertically from the forest floor up to 32 meters (Fig. 3) along a 48 m tall measurement tower. The 'j-BendAble Robust' OM3 fiber (j-fiber GmbH, Jena, Germany) had a translucent acrylic coating, and a diameter of 500μm. The FO cable was not extended beyond 32 meters due to the fragility of the thin cable. To hold it in place, it was connected to horizontal wooden beams which were extended from the measurement tower. The beams were placed every 4 meters, starting at the surface, increasing to every 2 meters from 26 m upward. The thin fiber was spliced to two different FO cables on both ends, which were routed down the tower, through the calibration baths and connected in a double-ended configuration to the DTS machine (van de Giesen et al., 2012). The thin-fiber temperature profile was measured from 21 August 2019 until 17 October 2019, when the FO cable broke.

The DTS machine used was a 2km range Ultima-S device (Silixa Ltd., UK). The measurement period was configured to 1 second per channel. This results in a double-ended calibrated temperature with an increased measurement period of ~2.3 s due to processing overhead. The raw data was calibrated using the python package 'dtscalibration' (des Tombe and Schilperoort, 2019).

The data was calibrated in a double-ended configuration, using a well-mixed bath at ambient temperature and a different bath maintained at 30 degrees Celsius. As the calibration was performed over splices, this could result in an offset and bias in the final temperatures (des Tombe et al., 2020). However, to detect strong temperature inversions we are mostly interested in the variations over air temperature over time and height, so a possible small bias in the absolute temperature is acceptable. DTS measurements suffer from inherent uncertainty in the measurements. With our Ultima-S device the expected measurement noise at the highest resolution has a standard deviation of $\sigma_{DTS} \approx 0.24$ K. By averaging in space and time this uncertainty can be reduced.
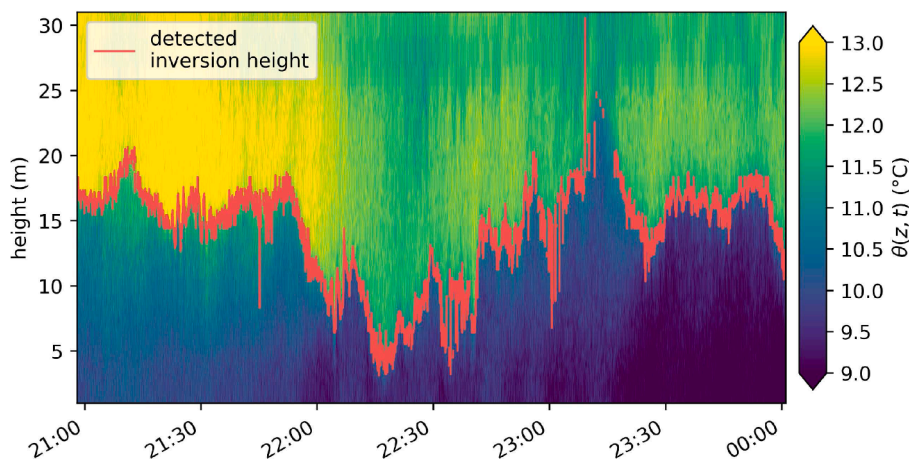
Fig. 4. Example of DTS measured potential temperature profile in time, along with the detected inversion height (where $\Delta\theta_{inv} > 1K$). Data of 14 September 2019. The 2D temperature plot has been smoothed using a Gaussian filter in time and space.

At the top of the measurement tower, at 48 m, an eddy covariance setup was placed consisting of a CSAT3 sonic anemometer (Campbell Sci., USA) and a LI7500 gas analyzer (LI-COR Biosciences, USA), both logged at 20 Hz. At 44 m a CNR4 Net Radiometer (Kipp & Zonen, the Netherlands) was placed, logging at 1 minute averages. On the forest floor, at ~0.8 m, a Young-81000 sonic anemometer (R.M. Young, USA) was placed, which was logged at 32 Hz. As this sonic anemometer did not have active heating, condensation on the transducers caused measurement disturbances on some nights. At 2 m another CNR4 Net Radiometer was set up, logging at 1 minute averages. All dates and times are in UTC.

2.3. Method

To be able to properly detect inversions within the DTS-measured temperature profiles we corrected all temperature values with the dry adiabatic lapse rate (i.e., $g\, c_p^{-1} \approx 9.68 \times 10^{-3}\, \mathrm{K\,m^{-1}}$ (Stull, 2015)), so as to get the potential temperature θ (K, in reference to the ground level), hereafter just referred to as temperature.

Preliminary inspection of temperatures learned that sharp inversion commonly occurred within the canopy. These inversions are characterized by a temperature jump of 1 - 2 K over a very small distance (< 0.3 m). For a general analysis we need a method to automatically detect the presence and features of these sharp inversions, such as the height at which the inversion is centered on (z_{inv}, m), and the strength (i.e., temperature jump) of the inversion ($\Delta\theta_{inv}$, K).

However, DTS measurements with high-frequency result in rather high measurement uncertainty, because statistical convergence decreases with decreasing averaging time. Uncertainty in the temperature will lead to difficulties in detecting inversions, when the signal ($\Delta\theta_{inv}$) to noise ratio is too small. To solve this, we used cross-correlation to detect step changes in the temperature profile. The cross-correlation between the temperature profile at a single measurement in time, and a sign function, is computed. The resulting data will show a local maximum value where a jump in temperature occurs. A detailed description and test of the method on synthetic data can be found in Appendix A.

For further data processing we chose a filter window size of 32 datapoints (corresponding to a physical filter window of 4 m), and a desired height detection accuracy of $\sigma(z_{inv}) < 1$ m. With this we could in theory detect sharp inversion layers down to a minimum strength of $\Delta\theta_{min} \approx 0.34$ K (see Appendix A).

After the height of a possible inversion is detected using the cross-correlation method, the temperature difference over the inversion can be determined. To do this, we calculate the difference between the temperature above (θ_{above}) and below (θ_{below}) the inversion height. To reduce the measurement uncertainty, we take the mean temperature in a range from 0.5 to 1.5 meters distance from the detected inversion height. The specific range is a compromise between reducing the uncertainty and how representative the data points are of the inversion strength.

$$\theta_{above} = \int_{z_{inv}+0.5}^{z_{inv}+1.5} \frac{\theta(z)}{\Delta z}\,dz, \quad \theta_{below} = \int_{z_{inv}-1.5}^{z_{inv}-0.5} \frac{\theta(z)}{\Delta z}\,dz, \quad (1)$$

where $\Delta z = 1$ m. The temperature difference over the inversion can then be calculated with;

$$\Delta\theta_{inv} = \theta_{above} - \theta_{below}. \quad (2)$$

Lastly, we performed a data screening. As the dataset is limited in time, a visual analysis of the temperature data can be performed to find events where, e.g., a sudden breakup of a strong inversion occurs, these events can then be studied in detail. In a preliminary look at the data, wave-like motions were clearly visible in the inversion height. These motions were visible in both the micro scale, as well as the submeso scale. We will analyze these events to describe their properties and discern their source.

3. Results and Discussion

3.1. Example inversion

As an illustration, Fig. 4 shows the potential temperature over height and time, as measured with DTS. The inversion height that was detected using the cross-correlation method is displayed over the temperature plot with a red line. During the night, the temperature along the entire profile falls gradually by about 2 K, both above and below the inversion layer. The local inversion has a strength of ~2 K, and varies a in height from 5 to 20 meters. Besides the larger changes in height, the inversion shows regular smaller oscillations of about 2 m at timescale of 1 – 2 minutes.

3.2. Inversion statistics

To correlate the presence of inversions with other variables, we define a persistent night as a night where more than 50% of the time an inversion with temperature strength greater than 0.5 K is present. An intermittent night is a night where 15 – 50% of the time such an inversion is present. 'Inversionless' nights are the remaining nights. Using these definitions, out of a total of 56 observed nights, persistent inversions (present for more than half of the night) were observed in 12 nights (21%). Twenty nights (36%) had some intermittent inversions, and the remaining 24 nights (43%) had no inversions within the canopy.
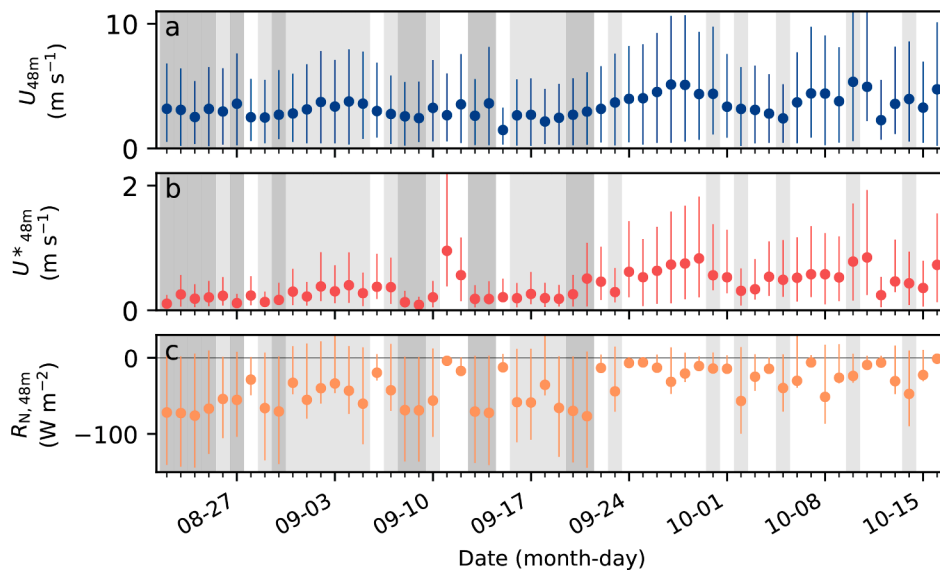
Fig. 5. Nighttime conditions during the measurement period of the wind speed at 48 meters (a), average friction velocity at 48 meters (b), and net radiation (c). The round markers denote the mean nighttime values, and the error bars the 25th and 75th percentiles. Nights with persistent inversions are shaded with dark gray, nights with intermittent inversions are shaded light gray.
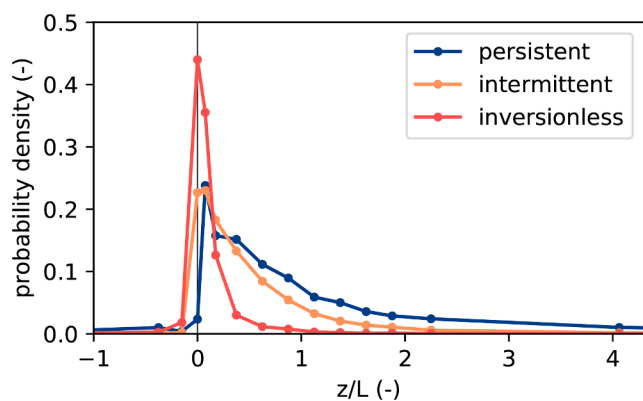

Fig. 6. Probability distribution functions of the stability parameter z/L for the three classes of nights.

These statistics indicate that the formation of inversion layers is a regular phenomenon, rather than an occasional event. The inversions were mostly present from 21 August 2019 to 23 September 2019, a period characterized by clear nights and low friction velocities (Fig. 5). During the last three weeks of the measurement period wind above the canopy was more turbulent and the sky was cloudy. Consequently, no inversions were detected during this period.

As the inversions seem to mostly occur during low-wind clear nights, it is likely that the atmospheric stability has a large influence on the formation of the inversions. To this end we compare the distribution of the stability parameter z/L of the three classes of nights (Fig. 6). This shows that inversionless nights have a mostly neutral value for z/L, intermittent nights can be neutral or stable, and nights with persistent inversions mostly have stable values for z/L.

Due to the mechanics of its formation and evolution, the inversion layer will be constrained by canopy morphology (PAI). Fig. 7 shows the distribution of the inversion layer over height, for two different inversion strengths. The stronger inversions are most likely to occur between 10 – 20 meters. Inversions were also regularly detected just above the forest floor (0 – 5 m) and near the canopy top (28 – 30 m). Within the overstory inversions are rare. It is likely that the dense branches reduce turbulent mixing, and thus, if there would be an inversion present within
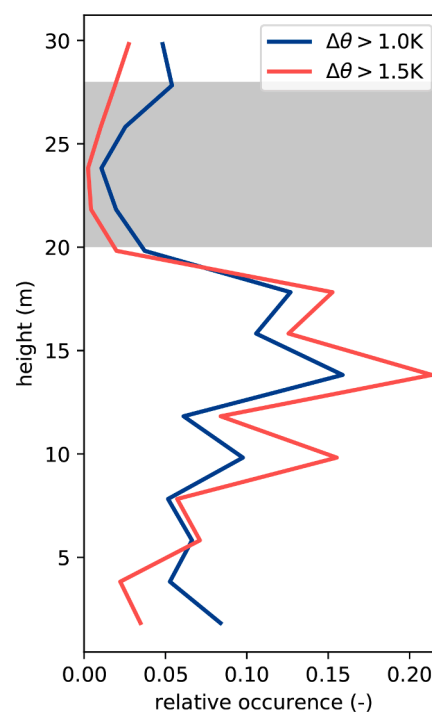
Fig. 7. Height at which inversions were detected, with two thresholds of minimum temperature differences; 1.0 K (red), and 1.5 K (blue). The gray shaded area shows the most dense part of the canopy.

the dense branches, the lack of mixing combined with the loss of heat due to radiative cooling would cause this layer to grow in height until it rises to the top of the canopy.

A reason for the preferential height could be that shear-driven mixing is enhanced both near the forest floor and just above and below the dense part of the canopy (at 20 – 26 m height). In forests with an open understory, a second wind speed maximum is often observed (Oliver, 1971; Shaw, 1977), which is accompanied by increased turbulence intensity and shear near the branches and forest floor (Baldocchi and Meyers, 1988). This enhanced shear results from the interaction

Fig. 8. Scatter plots of the nighttime friction velocity (a, c) or net radiation (b, d), and the inversion strength. Both above (a, b) and below the canopy (c, d).

Fig. 9. Data from an occurrence of a double inversion on 10 September 2019. Figure a shows the DTS temperature measurements from one point in time (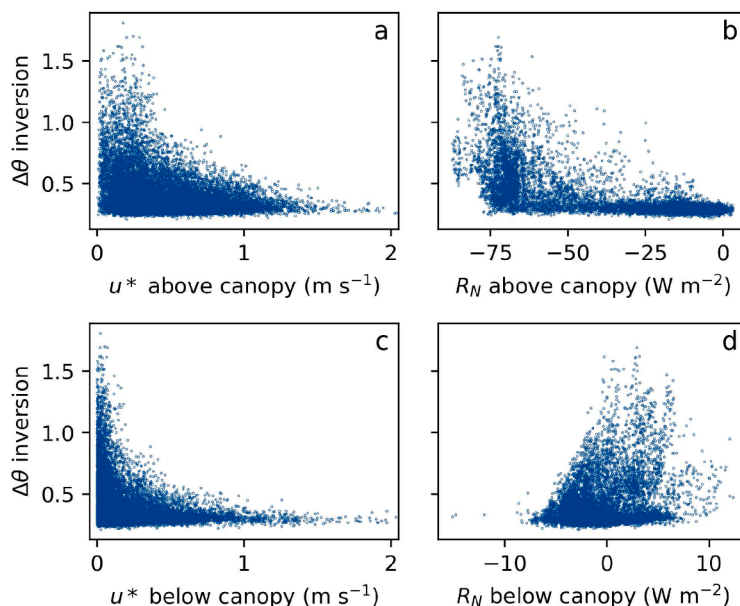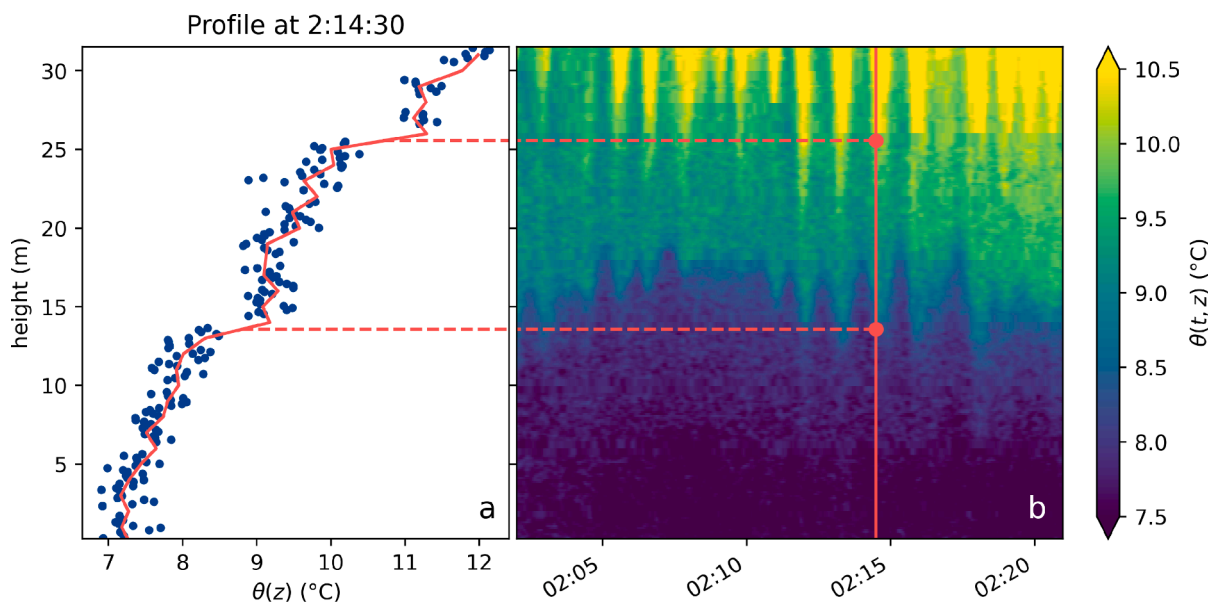2:14:30) in blue, with a 1 meter mean in red. The wide distribution of the blue data points is largely due to measurement noise. Figure b shows a color plot of the potential temperature in space and time.

between the wind and rigid (no-slip) surfaces such as the ground and the tree biomass at the top. This could result in a local minimum of the diffusivity between the forest floor and canopy. With the right conditions (i.e., the strength of the overall bulk inversion) this local minimum can exhibit a self-reinforcing effect, where the low diffusivity allows for a local sharpening of the temperature gradient, which in turn lowers the local turbulent diffusion. We analyzed the essence of this positive feedback, by a simple 1-D conceptual model in Section 4.

3.2.1. Formation of inversions

To study what could drive the formation of the inversions, the strength of the inversion is compared to the friction velocity and the net radiation, both above and below the canopy (Fig. 8). It is likely that these play a role, as a low friction velocity would allow the formation of

a stable stratification due to a lack of mixing, and a strong net radiative cooling would allow for large temperature differences.

As expected, the friction velocity above the canopy has to be low for a strong inversion to form or persist (Fig. 8a). The friction velocity below the canopy (Fig. 8c) shows an even stronger relationship, but causality cannot be derived from this as the presence of a strong inversion would cause a very low u_* value at 1 m height as well. The net radiation above the canopy also needs to be highly negative (Fig. 8b); meaning clear sky conditions with strong radiative cooling. However, interestingly, the net radiation below the canopy shows no clear relationship with the strength of the inversion (Fig. 8d). This could be due to the net radiation values being low, or that the radiometer near the forest floor is not a good indicator of the radiative cooling of the understory air. However, the placement of the radiometers do not allow us to descern between
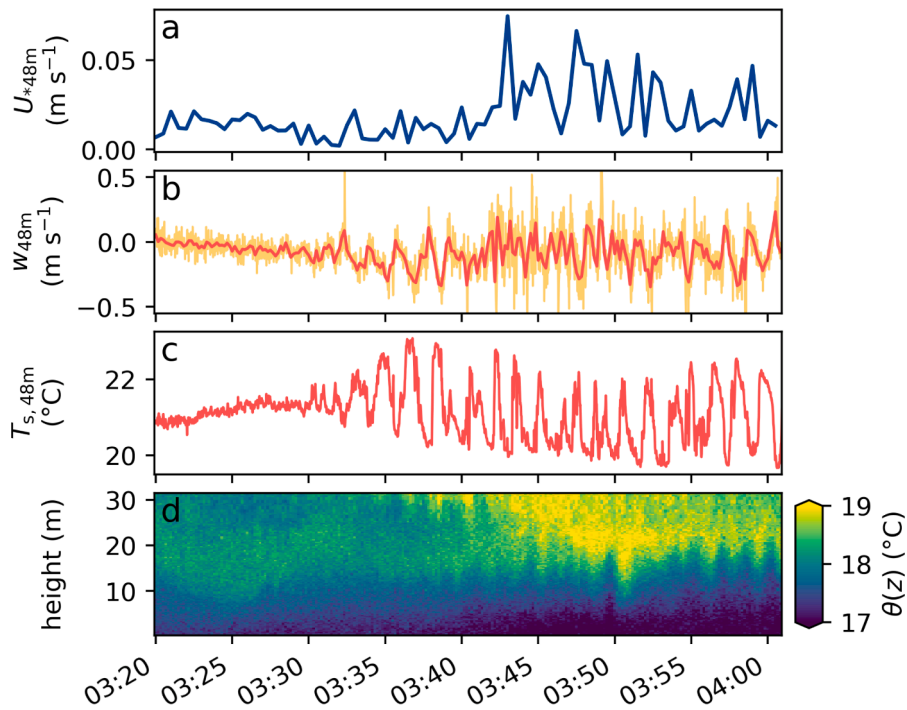
Fig. 10. Friction velocity above the canopy (a), 1 second mean vertical wind speed (b, in yellow), 5 second mean vertical wind speed (b, in red) above the canopy, sonic temperature above the canopy (c), and the DTS-measured temperature profile (d) during a wave-like event on 27 August 2019.
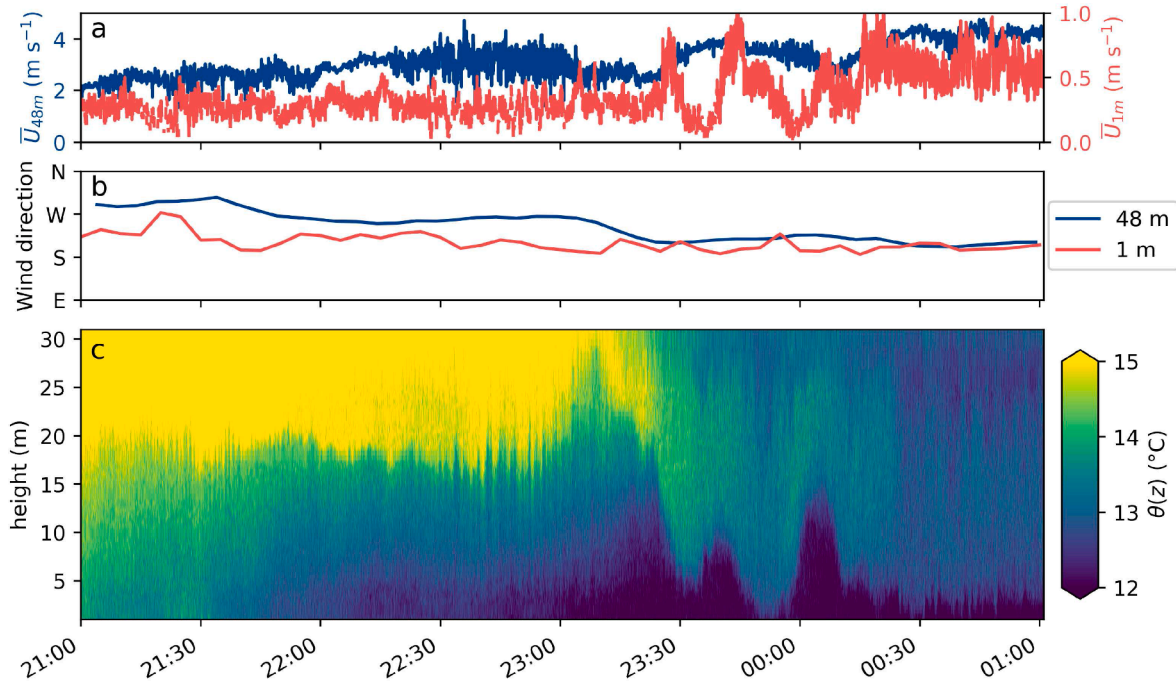
Fig. 11. Wind speed (a), wind direction (b) and temperature data (c) from the wave-like event on the night of 22 – 23 August 2019. Note that the wind speed (a) has two different scales for the two measurement heights. After an inversion at around 18 meters lasting until 23:00, a clear wavelike feature can be seen starting at 23:20, and lasting until 00:15.

cooling of the tree biomass and the understory air.

This lack of correlation between the inversion strength and the net radiation in the understory could mean that the source of the cold air under the inversion is not convective heat exchange with the cold forest floor. The cold air has to be supplied somehow however, either in the form of cold air plumes falling down from the top of the canopy (Dupont and Patton, 2012), by direct radiative cooling of the air, or a non-local

source of cold air (i.e. advection). It could also be that the net radiometer in the understory is located in a warm spot with less exposure to the open sky, and is therefore not fully representative of the whole understory.

3.2.2. Double inversions

On some occasions a double inversion was visible in the measured

Fig. 12. The formation of an inversion layer based on the 1-D model. a shows the initial conditions, b shows the onset of the collapse, and c shows the resulting inversion layer. The dashed orange line shows a profile with the maximum sustainable temperature gradient (see text). If the actual gradient is sharper than this theoretical limit a local inversion jump is formed.
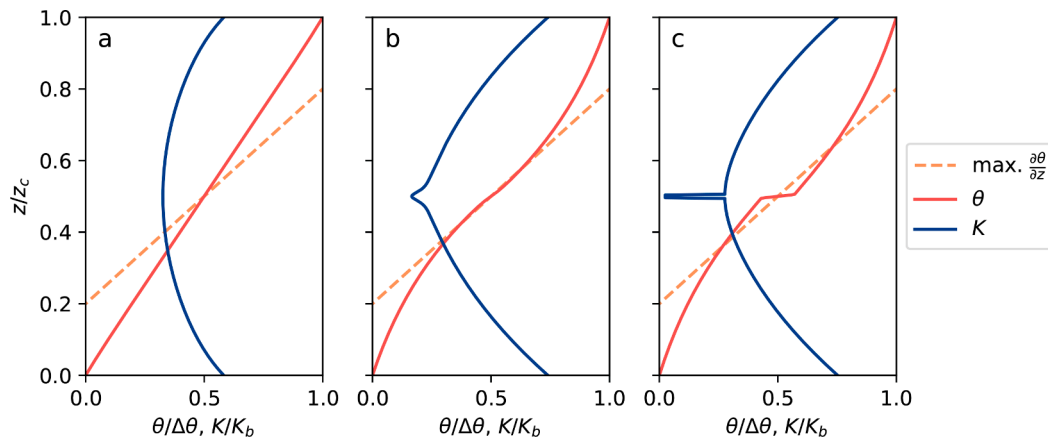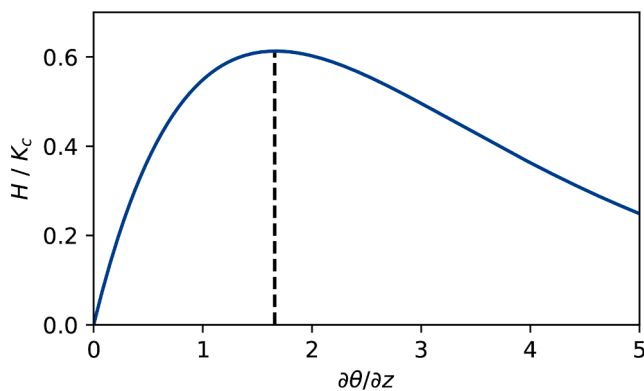

Fig. 13. The heat flux H (scaled by K_c), shown against the temperature gradient. With an increasing gradient, the heat flux will increase up to $\frac{\partial \theta}{\partial z} \approx$ ~1.67 K m^{-1}, after which the heat flux decreases with increasing gradient. The maximum sustainable heat flux is illustrated by the dashed line, which is at $\frac{\partial \theta}{\partial z} = \alpha^{-1}$ K m^{-1}

temperature profiles. An example of this is shown in Fig. 9. There are two clear temperature jumps visible in Fig. 9a, first at 14 m, and a second at 26 m. Both temperature jumps are ~1 K in magnitude. As can be seen in Fig. 9b, the inversions are not static in height, but oscillate with a period of about 80 seconds and an amplitude of 3 m. The two inversions seem to move in-phase, although small phase differences are small difficult to detect with the limited measurement frequency and the high measurement uncertainty. Due to the oscillations the top inversion dips in and out of view periodically; only when the inversion is below 32 meters it is measured. Even so, through manual inspection of the data double inversions were detected 16 of the nights, i.e., half of the nights where inversions were present. This is a minimum though, and it could even be that an upper inversion was present on all nights but remained out of the detection range. Therefore the inversion at the top of the canopy could be very common, but remains mostly undetected by the current DTS setup.

3.3. Wave-like motions of the inversion

On multiple days strong wave-like motions are visible in the inversion within the canopy. The motions have amplitudes between 2 and 10 meters, and a well-defined period of 50 – 100 seconds. These motions are alreayd visible in Fig. 9, both in the inversion at 15 meters, as well as the second inversion when it dips down to 30 meters. While the DTS

measurement noise makes it difficult to study the wave-like motions in detail, the motions are very clearly visible in the sonic anemometer data from the top of the measurement tower.

Wave-like motions with similar amplitudes and periods are frequently observed in atmospheric stably stratified layers of all kind. Recently, fascinating Kelvin-Helmholtz billows have been reported by e. g. echo sodargrams at Dome C in Antarctica (Petenko et al., 2019), where the homogeneous terrain and steady meteorological conditions allows detailed studies of the mechanics of the stable boundary layer. During the 'CHATS' experiment in a walnut orchard (Dupont and Patton, 2012) wave-like motions were visible during stable conditions as well, and were described as Kelvin-Helmholtz type structures. More specifically for forests, the observed motions could have their origin in 'linear canopy waves' (Cava et al., 2004), which form due to wind shear at the inflection point of the wind velocity profile above the canopy (Raupach et al., 1996; Finnigan, 2000; Hu et al., 2002). Flows with such inflection points are known to be hydrodynamically unstable (van der Linden et al., 2020; Kundu et al., 2016; Banta et al., 2007). Kelvin-Helmholtz structures are formed due to shear stress between two layers of different densities and these instabilities can dominate flow over uniform forest under very stable atmospheric conditions (Cava et al., 2004). Shear instabilities may quickly amplify and growing waves may become unstable and break (mixing events).

Fig. 10 shows a wave-like event on 22 August, where the absolute value of vertical wind speed at 48 m (Fig. 10b) was initially both small and steady, until an oscillating motion began. The amplification of this oscillation is clearly visible in the sonic temperature (Fig. 10c). However, after a few oscillations the vertical wind speed becomes more noisy, and the friction velocity increases (Fig. 10a). During this period of increased turbulence the air temperature in the overstory (20 – 30 m height) increases by over 1 K in less than 10 minutes (Fig. 10d). Seeing as this wave is likely generated above the canopy, has a monochromatic waveform with a period appropriate for canopy waves, and eventually breaks and generates a mixing event in the canopy (Finnigan, 2000; Hu et al., 2002), it is likely that the observed event results from canopy waves. The wave-like motions are visible in the inversion inside the canopy as well, as the vertical motion above the canopy is transferred into the canopy. Due to the low frequency of the motion, the canopy does not dampen the oscillations.

3.4. A wave-like submeso-scale motion

Besides the small scale wave motions, larger scale motions also occurred during the measurement campaign. Such submeso-scale motions can dominate the canopy flow dynamics and as such the correct

estimation of energy and mass fluxes during very stable conditions (Stefanello et al., 2020), especially in the lower part of the canopy (Santos et al., 2016; Oliveira et al., 2018). These motions have diverse origins such as horizontal meandering (Mahrt, 2007; Mortarini et al., 2019) or orthographicaly induced gravity waves (Corrêa et al., 2021), wave-like motions, and microfronts (Mahrt, 2010; Hoover et al., 2015)

On the night of 22 – 23 August 2019 a single wave like motion of significant amplitude was visible in the inversion height (Fig. 11). The event consisted of three sinusoidal disturbances in the height of a present inversion layer, with a time scale of ~20 minutes. During the disturbances the inversion changed height by 5 – 15 meters. The event was only detectable in the 1 m wind speed and the DTS temperature profile. The 3D wind speed measurements (u, w, v) at 48 m did not show any sign of the event. This might indicate that the disturbance is of advective origin rather than transported from above. Some signal of the event was visible in the sonic temperature at 48 m. Before and during the event the wind direction both above the canopy and at 1 m was ~200°(south-southwest).

The temperature decrease of the air under the inversion layer corresponds to a cooling rate of approximately 6 W m^{-2}, assuming no advection or mixing takes place. During the event there is no radiative cooling of the forest floor (~0 W m^{-2}), a negligible sensible heat flux at 1 m (3 W m^{-2}), and barely any ground heat flux (-2 W m^{-2}). While there is strong radiative cooling at the canopy top (-70 W m^{-2}), a top-down convective transport is somewhat unlikely due to the presence of the inversion. Thus it is likely that the source of the cold air is not local.

However, the slope at the site is approximately southeast (Appendix B), and the wind direction below the canopy is south-southwest. This would make it seem less likely that the origin of the event would be pulsating cold air drainage or density flows (Mahrt, 2007), as those would likely follow the direction of the slope.

3.5. Why could inversions within the canopy often elude detection?

While inversions within the canopy occurred frequently during this measurement campaign, it had not been clearly detected before at this site, both in studies without (Bosveld et al., 1999) as well as with DTS measurements (Schilperoort et al., 2018, 2020). In Schilperoort et al. (2020) it was inferred that some 'blocking layer' was present, but as armored DTS cables were used, the time response of the cable was insufficient to see a sharp inversion. The inversion often moves around and oscillates with a period of around 1 – 2 minutes. This makes detecting the presence of a sharp inversion difficult if the time response of the used sensors is longer than 15 – 30 seconds (1/4 of the period of the oscillations, to avoid aliasing).

Besides only time response, the vertical spatial resolution is also important in detecting the inversions. If DTS is used this is generally not a problem because these devices typically have a spatial resolution between 0.25 and 1 m. However, when using classical discrete sensors, the density of sensors can become an issue. A large amount of fast response sensors (e.g., fast-response thermocouples or sonic anemometers) would be required, one every ~2 m. For a subcanopy with a height of 20 meters this will quickly become a practical and financial issue.

Because detection of local inversions requires a very high measurement resolution, they are difficult to see with classic point sensors. This could mean this type of inversion is very common, but that they have thus far eluded detection.

4. Conceptual model for temperature-gradient sharpening

To test the hypothesis that layer formation is due to increased (turbulent) mixing near the canopy and forest floor, we created a conceptual model with the minimum ingredients to form a sharp inversion in the middle of the canopy. The 1-D numerical model describes the evolution of the (vertical) temperature profile with an effective turbulent diffusivity K;

$$\frac{\partial \theta}{\partial t} = \frac{\partial}{\partial z} K \frac{\partial \theta}{\partial z}, \tag{3}$$

where K is modeled by considering the effects of a constant background diffusivity (K_b), a stability correction, and a height-dependent correction in a dimensionless setting;

$$K_c = K_b \left(1 + 4 \frac{C_k}{z_c^2} (z(z - z_c)) \right), \tag{4}$$

which will create a parabolic profile, where z_c represents the height of the canopy, and C_k determines the minimal value (namely $(1 - C_k)K_b$) in the center of the profile. The parabolic profile is chosen to represent increased mixing at the ground surface and canopy crown compared to the trunk region, as wind shear is highest near the ground surface and canopy. Note that the surface flux is computed as $H = K \frac{\partial \theta}{\partial z}$. A stability correction is applied to K_c, to account for the suppression of mixing by stable stratification;

$$K = K_c e^{-\alpha \frac{\partial \theta}{\partial z}}, \tag{5}$$

with α as an inverse temperature-gradient scale, which controls the stability correction. For the numerical implementation a minimal diffusivity (K_{min}) is needed to prevent the diffusivity to approach 0. As the exact source of the cold air is unknown, and to simplify the model, a constant temperature difference of Δθ is maintained between the top (z = z_c) and bottom (z = 0) of the profile.

Eq. (3) is solved using the freely available Basilisk toolbox (Popinet, 2015), which contains a second-order accurate implicit-in-time finite-volume solver for the diffusion equation. Details of the setup can be found online (van Hooft and Schilperoort, 2021).

Fig. 12 shows how the inversion layer forms in the 1-D model. The temperature gradient in the center of the profile will become sharper, until the gradient matches the maximum sustainable value. After reaching this the system quickly collapses forming a discrete temperature change in the center of the profile. Values of C_k and α were tuned to generate layer formation.

In order to better understand the details of the presented conceptual system, we analyze the existence of steady-state solutions. A steady state solution is characterized by a heat flux which is constant over height. For a system that is not collapsed;

$$H = K \frac{\partial \theta}{\partial z} = K_c e^{-\alpha \frac{\partial \theta}{\partial z}} \cdot \frac{\partial \theta}{\partial z}, \tag{6}$$

which has a maximum gradient for $\frac{\partial \theta}{\partial z}(z = 0.5 \, z_c) = \alpha^{-1}$. With stronger temperature gradients the heat flux will decrease and the system will collapse, following the theory of maximum sustainable heat flux (Van de Wiel et al., 2012a,b). This concept is illustrated by Fig. 13, which shows the heat flux as a function of the temperature gradient. With an increasing gradient the heat flux reaches a maximum at $\partial \theta / \partial z = \alpha^{-1} = $ ~1.67 K m^{-1}, after which it decreases. At the left hand side of the maximum a negative feedback occurs: a larger temperature inversion result in a larger flux, which decreases the temperature contrast over the inversion. On the right hand side however, a positive feedback occurs: a stronger inversion decreases the heat flux, which results in a stronger inversion. The positive feedback is enabled by the non-linear dependency of K with respect to $\frac{\partial \theta}{\partial z}$.

As the height-average of $\partial \theta / \partial z$ is equal to $\langle \partial \theta / \partial z \rangle = \Delta \theta / z_c$, and the fact that the temperature gradient is strongest in the middle of the profile (z = $0.5 z_c$), we can derive that the system is always (mathematically) unstable when for the overall or bulk inversion;

$$\Delta \theta > \frac{z_c}{\alpha}, \tag{7}$$

and will collapse for any value of C_k. Higher values of α will cause the

system to collapse at a lower bulk $\Delta\theta$. Note that higher values of C_k can allow the collapse to occur before the bulk condition (Eq. (7)) is met. This is because a higher value of C_k allows K_c to become small locally. The local $\partial\theta/\partial z$ can then already reach the critical value of α^{-1} while the overall (bulk) gradient is modest and smaller than in Eq. (7). This is illustrated in Fig. 12b.

These results agree with our hypothesis and findings, and thus the simple model ingredients could hint at a potential mechanism for the formation of sharp inversions. However, this cannot be conclusively stated from this simplified model and with the available measurement data.

5. Conclusions and recommendations

This study demonstrated the presence of a previously not directly observed phenomenon; a spatially localized and highly dynamic inversion in the understory of a tall forest canopy. The presence of an inversion below the canopy will have a large effect on vertical transport of gasses such as carbon dioxide. The forest floor and soil are large sources of carbon dioxide, and any gas released at night during an inversion will not be transported vertically to the sensors above the canopy. The strong inversion was mostly present five to ten meters below the dense overstory, and formed during nights with strong radiative cooling and low friction velocities. The inversions did not build up from the forest floor. Instead, the source of the cold air was either cold air falling down from the canopy top or supplied through advection. However, in the locally measured temperature profile the air near the forest floor was generally $1 - 2$ K colder than the air in the canopy top, leaving advection as the most likely candidate.

A possible mechanic that could explain the formation of sharp inversions within the canopy could be a local minimum in the diffusivity. There is top-down mixing near the canopy top, and shear near the forest floor, while the middle of the understory is very bare. This mechanic was studied using a conceptual model with minimal ingredients, which gave results in line with the hypothesis. We found that a sharp inversion layer would always form within the canopy if the temperature difference between the forest floor and canopy top was large enough.

The inversion within the canopy was not the only one present. Above the canopy a second inversion regularly occurred, as would be expected under nocturnal conditions. Wave-like motions of this second inversion, likely linear canopy waves, induced waves in the inversion inside the canopy. These wave-like motions had a period of $50 - 100$ seconds, with an amplitude of at least $20 - 30$ meters above the canopy, and a reduced amplitude of $5 - 10$ meters within the canopy. Wave-like motions at larger scales were also detected. These submeso-scale motions were more transient and their source could not be conclusively determined.

While persistent temperature inversions within the canopy could be a feature specific to this study site, it is possible that this is a more regular feature in similarly structured canopies. Due to the vertical oscillations of the sharp inversion, sensors with a fast time response (better than $15 - 30$ seconds) have to be vertically distributed over the height of the canopy. Traditional temperature sensors do not respond fast enough, and sensors that do, like ultrasonic anemometers, are too costly to place at the required density. Due to these practical issues, features such as a sharp inversion within the canopy can often elude detection.

The fiber support structures did influence the data analysis, either when leaving them in (the fiber temperature will be affected by them), or when leaving gaps in the data. In follow up research a straddled support structure could be used to overcome this issue, where two stretches of optical fiber are placed in close proximity to each other without sharing the same support structure at the same heights. This would allow for a continuous temperature profile to be measured without gaps or artifacts. An increase in the number of fibers would also allow averaging them, thus lowering the measurement noise, allowing more subtle features to be detected.

By additionally using actively heated fiber optics, a continuous wind speed profile could be measured in addition to just the air temperature. The wind speed profile would aid in describing the interaction between the atmosphere and the canopy, as it would allow studying the wind shear, which is the driver of the turbulent mixing. To be able to study the wave-like features of the inversions in more detail, and to be able to conclusively determine their source, spatially distributed measurements, e.g., upstream and downstream of the tower, would additionally be required. With such a setup, it would be possible in the near future to finally explain the observed inversions and wave-like motions.

Author contributions

BS and CJR carried out the measurements. BS processed the data and performed the analysis. AH created and analyzed the conceptual model. BS prepared the manuscript with contributions from all authors.

Declaration of Competing Interest

The authors declare that they have no conflict of interest.

Acknowledgements

Appendix A: Inversion detection method

Block-difference method

The block-difference method uses a sliding window, where the difference in temperature between the top and the bottom of the window is computed. As the block-difference method does not make use of any data points between the top and bottom of the window, it is susceptible to white noise in the data. First smoothing the temperature profile with a Gaussian filter will significantly improve the method's accuracy, at the cost of losing data points on the edges of the profile.

Cross-correlation method

In the cross-correlation method (Rabiner and Gold, 1975), a sliding dot product is calculated between the vertical temperature profile and a step function (i.e., the sign/signum function):

$$\text{sgn}(n) = \begin{cases} -1, & \text{if } n < 0, \\ 0, & \text{if } n = 0, \\ 1, & \text{if } n > 0. \end{cases}$$

for $n = \left[-\frac{N}{2}, \frac{N}{2} \right]$ \hfill (A.1)

where N is the window size ($\mathbb{R}$) of the step function. The inversion height is determined to be at the height of the maximum value of the cross-
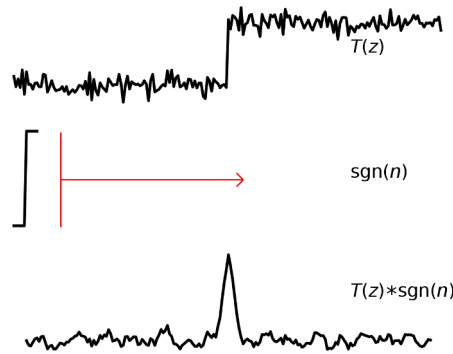
Fig. A.1. Example of the convolution of a synthetic temperature profile (T(z), with white noise) and the sign function, and the resulting cross-correlation. The detected height of the inversion is at the maximum value of the cross-correlation.
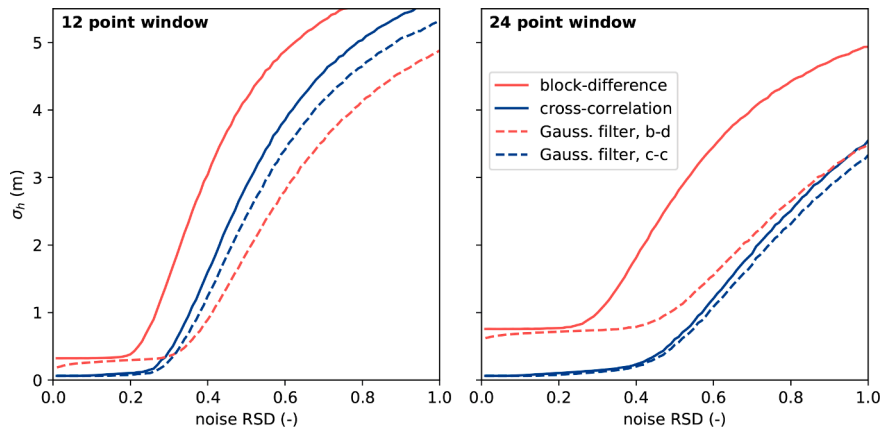

Fig. A.2. Uncertainty in the height detection of different inversion detection methods, compared to the relative standard deviation (RSD) of the noise. The block-difference method is compared to the cross-correlation method, and both methods are compared after using a Gaussian filter ($\sigma = 1$) to smooth out the measurement noise.

correlation (Fig. A.1).

Test on synthetic data

As a way to test the performance of the different detection methods, a synthetic profile was generated. The profile has a 1 K temperature step halfway up the profile. White noise was added to this synthetic profile, with different scales to assess the performance of the different methods over a range of signal-to-noise ratios. The profile was chosen to have 200 data points, corresponding to a ~25 m profile with the vertical resolution of the Ultima-S DTS. Performance of all detection algorithms will degrade with an increased profile size, as random noise becomes more likely to resemble a step change.

To compare the effect the window size has, we show the results of a window size of 12 and 24 points, corresponding to a physical window size of ~1.5 and 3 meters respectively (for the Ultima-S DTS). Larger window sizes will not be able to detect a step change in the bottom or top N/2 data points of the profile (without padding the data), as the convolution requires a minimum amount of data points equal to the window size N.

Noise removal with a Gaussian filter can improve the detection methods, therefore the detection methods were also applied to the profile data filtered with a Gaussian filter with $\sigma = 1$.

Fig. A.2 shows the performance of the inversion detection methods in the form of the standard deviation of detected height (σ_h) compared to the relative standard deviation (RSD) of the noise. The RSD is defined as ratio of the standard deviation of the noise compared to the signal size (i.e., the temperature jump). By running a large number of simulations any random variation is removed. The bias is near-zero in all methods.

The cross-correlation method seems to outperform the block-difference in all cases, except when the window size is very small, and the noise level is very high. While the performance of the cross-correlation method improves dramatically as the window size improves, the block-difference method works best at more modest window sizes. First applying a Gaussian filter will see most improvement in the block-difference method, while the cross-correlation method is barely affected by it.

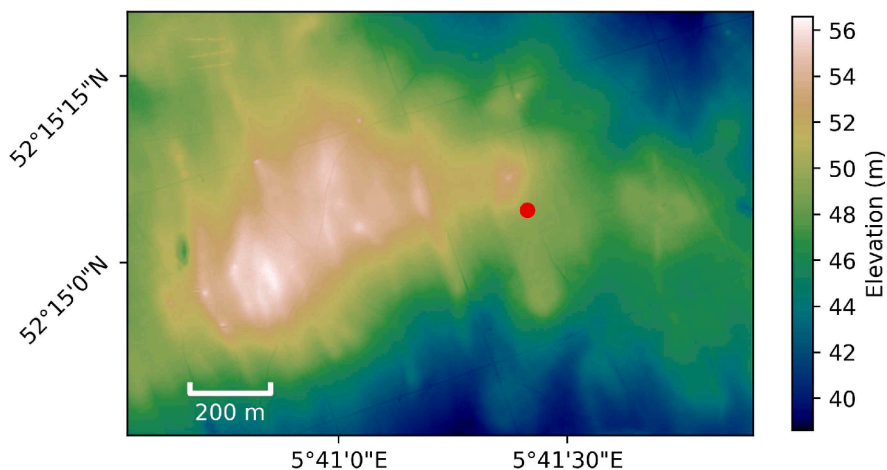**Appendix B: Height map Speulderbos**

Fig. B.1

Fig. B.1. Height map of the area surrounding the measurement site. Based on the open data of 'Actueel Hoogtebestand Nederland 3' (AHN3). The red marker shows the location of the measurement tower.

Appendix C: Speulderbos plant area index profile

The vertical profile of the plant area index (PAI) at the research site was previously determined using 10 images distributed over the height of the canopy, for 3 sides of the tower (Schilperoort et al., 2020). The images were processed using Gap Light Analyser (Frazer et al., 1999). The bottom 20 m of the forest is completely bare, except from the tree stems. The bulk of the branches are located around 22 to 28 m height (Fig. C.1).
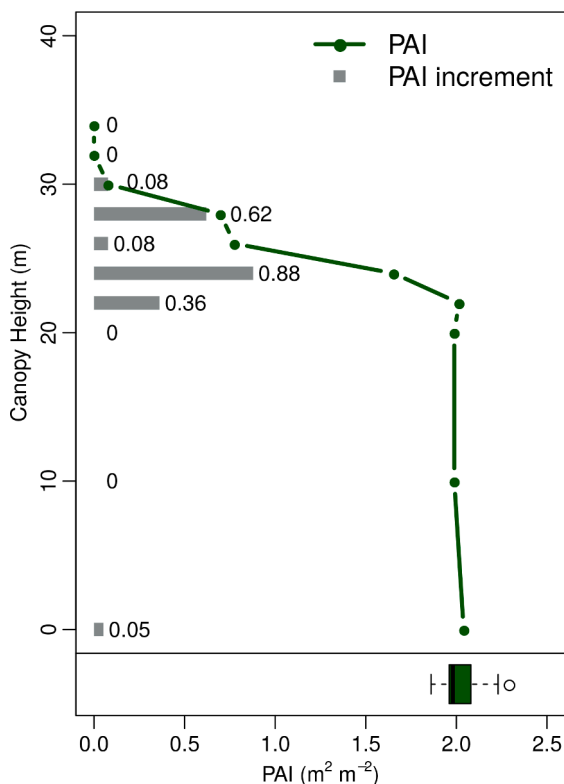

Fig. C.1. Profile of the plant area index (PAI) at the Speulderbos site (Schilperoort et al., 2020).

References

Alekseychik, P., Mammarella, I., Launiainen, S., Rannik, Ü., Vesala, T., 2013. Evolution of the nocturnal decoupled layer in a pine forest canopy. Agricultural and Forest Meteorology 174-175, 15–27. https://doi.org/10.1016/j.agrformet.2013.01.011.

Aubinet, M., Feigenwinter, C., Heinesch, B., Laffineur, Q., Papale, D., Reichstein, M., Rinne, J., van Gorsel, E., 2012. Nighttime Flux Correction. Eddy Covariance: A Practical Guide to Measurement and DataAnalysis. Springer, Dordrecht/Heidelberg/London/New York, pp. 133–157 edited by Aubinet, M., Vesala, T., and Papale, D.

Baldocchi, D.D., Meyers, T.P., 1988. Turbulence structure in a deciduous forest. Boundary-Layer Meteorology 43, 345–364. https://doi.org/10.1007/BF00121712.

Banta, R.M., Mahrt, L., Vickers, D., Sun, J., Balsley, B.B., Pichugina, Y.L., Williams, E.J., 2007. The Very Stable Boundary Layer on Nights with Weak Low-Level Jets. Journal of the Atmospheric Sciences 64, 3068–3090. https://doi.org/10.1175/JAS4002.1.

Barr, A.G., King, K.M., Gillespie, T.J., Den Hartog, G., Neumann, H.H., 1994. A comparison of bowen ratio and eddy correlation sensible and latent heat flux measurements above deciduous forest. Boundary-Layer Meteorology 71, 21–41. https://doi.org/10.1007/BF00709218.

Barr, A.G., Richardson, A.D., Hollinger, D.Y., Papale, D., Arain, M.A., Black, T.A., Bohrer, G., Dragoni, D., Fischer, M.L., Gu, L., Law, B.E., Margolis, H.A., Mccaughey, J.H., Munger, J.W., Oechel, W., Schaeffer, K., 2013. Use of change-point detection for friction-velocity threshold evaluation in eddy-covariance studies. Agricultural and Forest Meteorology 171-172, 31–45. https://doi.org/10.1016/j.agrformet.2012.11.023.

Bosveld, F.C., Holtslag, A.A., Van Den Hurk, B.J., 1999. Nighttime convection in the interior of a dense Douglas fir forest. Boundary-Layer Meteorology 93, 171–195. https://doi.org/10.1023/A:1002039610790.

Cava, D., Katul, G.G., 2009. The Effects of Thermal Stratification on Clustering Properties of Canopy Turbulence. Boundary-Layer Meteorology 130, 307–325. https://doi.org/10.1007/s10546-008-9342-6.

Cava, D., Giostra, U., Siqueira, M., and Katul, G.: Organised Motion and Radiative Perturbations in the, Boundary-Layer Meteorology, 112, 129–157, doi:10.1023/B:BOUN.0000020160.28184.a0, 2004.

Cisneros Vaca, C., Ghimire, C.P., van der Tol, C., 2018. Spatial Patterns and Temporal Stability of Throughfall in a Mature Douglas-fir Forest. Water 10. https://doi.org/10.3390/w10030317.

Corrêa, P.B., Dias-Júnior, C.Q., Cava, D., Sörgel, M., Botía, S., Acevedo, O., Oliveira, P.E., Ocimar Manzi, A., Toledo Machado, L.A., dos Santos Martins, H., Tsokankunku, A., de Araújo, A.C., Lavric, J.V., Walter, D., Mortarini, L., 2021. A case study of a gravity wave induced by Amazon forest orography and low level jet generation. Agricultural and Forest Meteorology 307, 108 457. https://doi.org/10.1016/j.agrformet.2021.108457.

des Tombe, B., Schilperoort, B., Bakker, M., 2020. Estimation of Temperature and Associated Uncertainty from Fiber-Optic Raman-Spectrum Distributed Temperature Sensing. Sensors 20, 2235. https://doi.org/10.3390/s20082235.

des Tombe, B. F. and Schilperoort, B.: Python distributed temperature sensing calibration, doi:10.5281/zenodo.3531558, 2019.

Dupont, S., Patton, E.G., 2012. Momentum and scalar transport within a vegetation canopy following atmospheric stability and seasonal canopy changes: The CHATS experiment. Atmospheric Chemistry and Physics 12, 5913–5935. https://doi.org/10.5194/acp-12-5913-2012.

Finnigan, J., 2000. Turbulence in Plant Canopies. Annual Review of Fluid Mechanics 32, 519–571. https://doi.org/10.1146/annurev.fluid.32.1.519.

Fitzjarrald, D.R., Moore, K.E., 1990. Mechanisms of nocturnal exchange between the rain forest and the atmosphere. Journal of Geophysical Research 95 (16), 839. https://doi.org/10.1029/JD095iD10p16839.

Frazer, G.W., Canham, C., Lertzman, K., 1999. Gap Light Analyzer (GLA), Version 2.0: Imaging software to extract canopy structure and gap light transmission indices from true-colour fisheye photographs, users manual and program documentation. Simon Fraser University, Burnaby, British Columbia, and the Institute of Ecosystem Studies. Millbrook, New York.

Göckede, M., Thomas, C., Markkanen, T., Mauder, M., Ruppert, J., Foken, T., 2007. Sensitivity of Lagrangian Stochastic footprints to turbulence statistics. Tellus, Series B: Chemical and Physical Meteorology 59, 577–586. https://doi.org/10.1111/j.1600-0889.2007.00275.x.

Goulden, M.L., Munger, J.W., Fan, S.-M., Daube, B.C., Wofsy, S.C., 1996. Measurements of carbon sequestration by long-term eddy covariance: methods and a critical evaluation of accuracy. Global Change Biology 2, 169–182. https://doi.org/10.1111/j.1365-2486.1996.tb00070.x.

Hartog, A.H., 2017. An Introduction to Distributed Optical Fibre Sensors. CRC Press, Boca Raton, Florida. https://doi.org/10.1201/9781315119014.

Hoover, J.D., Stauffer, D.R., Richardson, S.J., Mahrt, L., Gaudet, B.J., Suarez, A., 2015. Submeso Motions within the Stable Boundary Layer and Their Relationships to Local Indicators and Synoptic Regime in Moderately Complex Terrain. Journal of Applied Meteorology and Climatology 54, 352–369. https://doi.org/10.1175/JAMC-D-14-0128.1.

Hu, X., Lee, X., Stevens, D.E., Smith, R.B., 2002. A Numerical Study Of Nocturnal Wavelike Motion In Forests. Boundary-Layer Meteorology 102, 199–223. https://doi.org/10.1023/A:1013167228992.

Izett, J. G., Schilperoort, B., Coenders-Gerrits, M., Baas, P., Bosveld, F. C., and van de Wiel, B. J. H.: Missed Fog?, Boundary-Layer Meteorology, 173, 289–309, doi:10.1007/s10546-019-00462-3, 2019.

Jocher, G., Ottosson Löfvenius, M., De Simon, G., Hörnlund, T., Linder, S., Lundmark, T., Marshall, J., Nilsson, M.B., Näsholm, T., Tarvainen, L., Öquist, M., Peichl, M., 2017. Apparent winter CO2 uptake by a boreal forest due to decoupling. Agricultural and Forest Meteorology 232, 23–34. https://doi.org/10.1016/j.agrformet.2016.08.002.

Jocher, G., Fischer, M., Šigut, L., Pavelka, M., Sedlák, P., Katul, G., 2020. Assessing decoupling of above and below canopy air masses at a Norway spruce stand in complex terrain. Agricultural and Forest Meteorology 294, 108 149. https://doi.org/10.1016/j.agrformet.2020.108149.

Katul, G., Goltz, S.M., Hsieh, C.I., Cheng, Y., Mowry, F., Sigmon, J., 1995. Estimation of surface heat and momentum fluxes using the flux-variance method above uniform and non-uniform terrain. Boundary-Layer Meteorology 74, 237–260. https://doi.org/10.1007/BF00712120.

Kundu, P.K., Cohen, I.M., Dowling, D.R., 2016. Turbulence, in: Fluid Mechanics. Elsevier 603–697. https://doi.org/10.1016/B978-0-12-405935-1.00012-5.

Lapo, K., Freundorfer, A., Pfister, L., Schneider, J., Selker, J., Thomas, C., 2020. Distributed observations of wind direction using microstructures attached to actively heated fiber-optic cables. Atmospheric Measurement Techniques 13, 1563–1573. https://doi.org/10.5194/amt-13-1563-2020.

Mahrt, L., 2007. Weak-wind mesoscale meandering in the nocturnal boundary layer. Environmental Fluid Mechanics 7, 331–347. https://doi.org/10.1007/s10652-007-9024-9.

Mahrt, L., 2010. Common microfronts and other solitary events in the nocturnal boundary layer. Quarterly Journal of the Royal Meteorological Society 136, 1712–1722. https://doi.org/10.1002/qj.694.

Mortarini, L., Cava, D., Giostra, U., Costa, F.D., Degrazia, G., Anfossi, D., Acevedo, O., 2019. Horizontal Meandering as a Distinctive Feature of the Stable Boundary Layer. Journal of the Atmospheric Sciences 76, 3029–3046. https://doi.org/10.1175/JAS-D-18-0280.1.

Oliveira, P.E.S., Acevedo, O.C., Sörgel, M., Tsokankunku, A., Wolff, S., Araújo, A.C., Souza, R.A.F., Sá, M.O., Manzi, A.O., Andreae, M.O., 2018. Nighttime wind and scalar variability within and above an Amazonian canopy. Atmospheric Chemistry and Physics 18, 3083–3099. https://doi.org/10.5194/acp-18-3083-2018.

Oliver, H.R., 1971. Wind profiles in and above a forest canopy. Quarterly Journal of the Royal Meteorological Society 97, 548–553. https://doi.org/10.1002/qj.49709741414.

Papale, D., Reichstein, M., Aubinet, M., Canfora, E., Bernhofer, C., Kutsch, W., Longdoz, B., Rambal, S., Valentini, R., Vesala, T., Yakir, D., 2006. Towards a standardized processing of Net Ecosystem Exchange measured with eddy covariance technique: Algorithms and uncertainty estimation. Biogeosciences 3, 571–583. https://doi.org/10.5194/bg-3-571-2006.

Peltola, O., Lapo, K., Martinkauppi, I., O'Connor, E., Thomas, C.K., Vesala, T., 2020. Suitability of fiber-optic distributed temperature sensing to reveal mixing processes and higher-order moments at the forest-air interface. Atmospheric Measurement Techniques Discussions 1–31.

Petenko, I., Argentini, S., Casasanta, G., Genthon, C., and Kallistratova, M.: Stable Surface-Based Turbulent Layer During the Polar Winter at Dome C, Antarctica: Sodar and In Situ Observations, Boundary-Layer Meteorology, 171, 101–128, doi:10.1007/s10546-018-0419-6, 2019.

Popinet, S., 2015. A quadtree-adaptive multigrid solver for the Serre–Green–Naghdi equations. Journal of Computational Physics 302, 336–358. https://doi.org/10.1016/j.jcp.2015.09.009.

Rabiner, L.R., Gold, B., 1975. Theory and application of digital signal processing. Prentice Hall, Englewood Cliffs, NJ.

Raupach, M.R., Finnigan, J.J., Brunei, Y., 1996. Coherent eddies and turbulence in vegetation canopies: The mixing-layer analogy. Boundary-Layer Meteorology 78, 351–382. https://doi.org/10.1007/BF00120941.

Santos, D.M., Acevedo, O.C., Chamecki, M., Fuentes, J.D., Gerken, T., Stoy, P.C., 2016. Temporal Scales of the Nocturnal Flow Within and Above a Forest Canopy in Amazonia. Boundary-Layer Meteorology 161, 73–98. https://doi.org/10.1007/s10546-016-0158-5.

Schilperoort, B., Coenders-Gerrits, M., Luxemburg, W., Rodríguez, C.J., Vaca, C.C., Savenije, H., 2018. Technical note: Using distributed temperature sensing for Bowen ratio evaporation measurements. Hydrology and Earth System Sciences 22, 819–830. https://doi.org/10.5194/hess-22-819-2018.

Schilperoort, B., Coenders-Gerrits, M., Jiménez Rodriguez, C., van der Tol, C., van de Wiel, B., Savenije, H., 2020. Decoupling of a Douglas fir canopy: a look into the subcanopy with continuous vertical temperature profiles. Biogeosciences Discussions 1–25. https://doi.org/10.5194/bg-2020-216.

Shaw, R.H., 1977. Secondary Wind Speed Maxima Inside Plant Canopies. Journal of Applied Meteorology 16, 514–521 doi:10.1175/1520-0450(1977)016<0514:SWSMIP>2.0.CO;2.

Smolen, J.J., van der Spek, A., 2003. Distributed Temperature Sensing A DTS Primer for Oil & Gas Production, Shell International Exploration and Production. The Hague, The Netherlands, p. 97.

Stefanello, M., Cava, D., Giostra, U., Acevedo, O., Degrazia, G., Anfossi, D., Mortarini, L., 2020. Influence of submeso motions on scalar oscillations and surface energy balance. Quarterly Journal of the Royal Meteorological Society 146, 889–903. https://doi.org/10.1002/qj.3714.

Stull, R., 2015. Practical Meteorology - An Algebra-based Survey of Atmospheric Science. Department of Earth, Ocean & Atmospheric Sciences, University of British Columbia, Vancouver, BC. https://doi.org/10.14288/1.0300441.

Thomas, C. K., Kennedy, A. M., Selker, J. S., Moretti, A., Schroth, M. H., Smoot, A. R., Tufillaro, N. B., and Zeeman, M. J.: High-Resolution Fibre-Optic Temperature Sensing: A New Tool to Study the Two-Dimensional Structure of Atmospheric Surface-Layer Flow, Boundary-Layer Meteorology, 142, 177–192, doi:10.1007/s10546-011-9672-7, 2012.

Thomas, C.K., Martin, J.G., Law, B.E., Davis, K., 2013. Toward biologically meaningful net carbon exchange estimates for tall, dense canopies: Multi-level eddy covariance observations and canopy coupling regimes in a mature Douglas-fir forest in Oregon.

Agricultural and Forest Meteorology 173, 14–27. https://doi.org/10.1016/j.agrformet.2013.01.001.

Thomas, C.K., Serafimovich, A., Siebicke, L., Gerken, T., Foken, T., 2017. Coherent Structures and Flux Coupling, in: Energy and Matter Fluxes of a Spruce Forest Ecosystem. Springer International Publishing 113–135. https://doi.org/10.1007/978-3-319-49389-3_6.

van de Giesen, N., Steele-Dunne, S.C., Jansen, J., Hoes, O., Hausner, M.B., Tyler, S., Selker, J., 2012. Double-Ended Calibration of Fiber-Optic Raman Spectra Distributed Temperature Sensing Data. Sensors 12, 5471–5485. https://doi.org/10.3390/s120505471.

Van de Wiel, B.J.H., Moene, A.F., Jonker, H.J.J., 2012. The Cessation of Continuous Turbulence as Precursor of the Very Stable Nocturnal Boundary Layer. Journal of the Atmospheric Sciences 69, 3097–3115. https://doi.org/10.1175/JAS-D-12-064.1.

Van de Wiel, B.J.H., Moene, A.F., Jonker, H.J.J., Baas, P., Basu, S., Donda, J.M.M., Sun, J., Holtslag, A.A.M., 2012. The Minimum Wind Speed for Sustainable Turbulence in the Nocturnal Boundary Layer. Journal of the Atmospheric Sciences 69, 3116–3127. https://doi.org/10.1175/JAS-D-12-0107.1.

van der Linden, S.J., van de Wiel, B.J., Petenko, I., van Heerwaarden, C.C., Baas, P., Jonker, H.J., 2020. A businger mechanism for intermittent bursting in the stable boundary layer. Journal of the Atmospheric Sciences 77, 3343–3360. https://doi.org/10.1175/JAS-D-19-0309.1.

van Hooft, A. and Schilperoort, B.: Temperature-gradient sharpening in a canopy, URL http://www.basilisk.fr/sandbox/Antoonvh/canopy.c, 2021.

van Ramshorst, J.G.V., Coenders-Gerrits, M., Schilperoort, B., van de Wiel, B.J.H., Izett, J.G., Selker, J.S., Higgins, C.W., Savenije, H.H.G., van de Giesen, N.C., 2019. Wind speed measurements using distributed fiber optics: a windtunnel study. Atmospheric Measurement Techniques Discussions 1–21. https://doi.org/10.5194/amt-2019-63.

Wilson, K., 2002. Energy balance closure at FLUXNET sites. Agricultural and Forest Meteorology 113, 223–243. https://doi.org/10.1016/S0168-1923(02)00109-0.

Zeeman, M.J., Selker, J.S., Thomas, C.K., 2015. Near-Surface Motion in the Nocturnal, Stable Boundary Layer Observed with Fibre-Optic Distributed Temperature Sensing. Boundary-Layer Meteorology 154, 189–205. https://doi.org/10.1007/s10546-014-9972-9.